Heavy Oil Production by Electromagnetic Heating in Hydraulically Fractured Wells

ARTICLE *in* ENERGY & FUELS · SEPTEMBER 2014

Impact Factor: 2.79 · DOI: 10.1021/ef5014264

3 AUTHORS:

Alfred Ya. Davletbaev
Bashkir State University
32 PUBLICATIONS **60** CITATIONS
SEE PROFILE

L. A. Kovaleva
Bashkir State University
40 PUBLICATIONS **101** CITATIONS
SEE PROFILE

Tayfun Babadagli
University of Alberta
249 PUBLICATIONS **1,689** CITATIONS
SEE PROFILE

energy&fuels

Article

pubs.acs.org/EF

Heavy Oil Production by Electromagnetic Heating in Hydraulically Fractured Wells

Alfred Davletbaev,[†] Liana Kovaleva,[†] and Tayfun Babadagli*[,‡]

[†]Department of Applied Physics, Bashkir State University, Ufa 450074, Russia

[‡]Department of Civil and Environmental Engineering, School of Mining and Petroleum Engineering, University of Alberta, Edmonton, Alberta T6G 2W2, Canada

ABSTRACT: The results of numerical studies of heavy oil production by radio frequency−electromagnetic heating (RF−EM) from hydraulically fractured low-permeability reservoirs are presented. The fluid flow to a single vertical high-conductivity fracture is considered assuming that electrical and thermal properties of the reservoir rock and fluid-saturated fracture are the same. Comparative analysis is performed for the cases of heavy oil recovery by RF−EM radiation with hydraulic fracturing and "cold" production. Modeling of the combined multi-stage method and economic analysis for different RF−EM generator powers, differential pressure between the well and formation, and the fracture conductivity showed that the method is most effective for wells with "short" and low-conductivity hydraulic fractures.

1. INTRODUCTION

The investigations on the possibility of applying a high-frequency electromagnetic field to stimulate wells dates back to the early 1970s. Chistyakov et al. studied wellbore heating using electromagnetic sources experimentally.[1] Later, Sayakhov described the physical fundamentals of fluid flow under a radio frequency−electromagnetic heating (RF−EM) field.[2] In that paper, the results of experimental studies of filtration in a high-frequency field were presented. The way to determine the RF−EM impact on some characteristics, such as flow rate and temperature, in the reservoir model was also shown.

Chakma and Jha performed laboratory experiments on a physical model using one horizontal well for gas injection and one horizontal well for oil production in the model.[3] They introduced electromagnetic energy into the model by two electrodes. Kasevich et al. conducted experimental laboratory studies using an EM power source of 0.2 and 1 kW. During one of the experiments, a core sample of Bakersfield field was heated to 150 °C in 49 min with a transmitter power of 0.4 kW.[4] More recently, Ovalles et al. used the microwave power of 0.65 kW to heat core samples saturated with different viscosity heavy oils [25° and 7.7° American Petroleum Institute (API) gravity]. The experimental results were applied to a mathematical model to predict the recovery potential of three oil deposits in Venezuela.[5]

Solvent was involved in the EM heating studies published over the past decade. Nigmatulin et al. reviewed the results of laboratory studies on injection solvent combined with RF−EM heating.[6] On the basis of these laboratory experiments, model studies were performed by Davletbaev et al. to investigate the application field scale.[7,8] Kovaleva et al. analyzed the results of experimental studies of the effects of RF−EM fields on a multicomponent filtration in porous media as well as the effect of the EM field on the adsorption processes of heavy oil.[9] They also analyzed polar components of the structure by scanning atomic force microscopy. Increasing oil prices led the researchers to spend more efforts in the area of EM heating as an alternative method of heavy oil recovery.[10−14]

It is known that RF electromagnetic irradiation allows heat into the formation, regardless of its reservoir properties, by creating volumetric heat sources in the formation. The penetration of thermal heating can be in the order of tens of meters.[15,16] For example, in field tests on the Sugushlinskaya bitumen area in the Russian Federation, 32 h of RF−EM irradiation at a power generator of 60 kW resulted in an increase in the temperature in the well up to 310 °C. In the observation well located at a distance of 5 m from this well showed a 45 °C increase in the temperature.[16] Similar field tests were carried out in Bakersfield, CA.[4] After 20 h of RF−EM irradiation (generator power of 25 kW, frequency of 13.56 MHz, and depth of the reservoir of 620 ft), temperature increased to 120 °C in the observation well at a distance of 10 ft from the well with the generator. On the other hand, the production of heavy oil from the formations with low permeability may be economically inefficient. One solution in this type of field is hydraulic fracturing, but flow rates are typically very low and decay rapidly during "cold" production of heavy oil. Steam injection in low-permeability reservoirs is usually ineffective, especially in deep sediments. This requires further investigations on new ideas to develop such heavy oil deposits.

In this paper, we consider the possibility of using combined technologies of RF radiation of EM waves and hydraulic fracturing in deep and low-permeability heavy oil deposits and propose a multi-stage combined technology. The first stage (after hydraulic fracturing) is "cold" oil production. In the second stage, oil production continues with simultaneous RF−EM irradiation. In the third stage, oil production is carried out with the generator off (i.e., generator is stopped temporarily) until the temperature in the well drops to the initial value of the formation temperature. The duration of the third stage can be

Received: June 26, 2014
Revised: August 27, 2014
Published: August 28, 2014

dx.doi.org/10.1021/ef5014264 | *Energy Fuels* 2014, 28, 5737−5744

determined on the basis of the reduction of the temperature and/or oil production to infeasible values. If necessary, this process (second and third stages) can be performed cyclically. We first define a mathematical model of this multi-stage process and perform sensitivity analyses.

2. FORMULATION OF THE PROBLEM AND BASIC EQUATIONS

2.1. Definition of the Model. This paper presents a two-dimensional mathematical model of heavy oil production by multi-stage combined technology of RF−EM irradiation at the bottom zone of the production well that is hydraulically fractured. Figure 1 shows

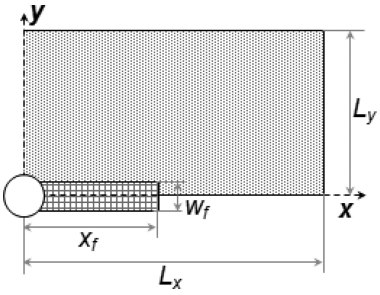

Figure 1. Schematic of a fractured well.

the geometry of the problem. The mathematical model of the problem reduces to a system of equations for the pressure and temperature in the fracture ($0 \le x \le x_f$, $0 \le y \le w_f/2$)

$$\phi_f \beta_{ft} \frac{\partial P_f}{\partial t} = \frac{\partial}{\partial x}\left(\frac{k_f}{\mu_o}\frac{\partial P_f}{\partial x}\right) + \frac{q}{w_f h} \tag{1}$$

$$\alpha_{ft}\frac{\partial T_f}{\partial t} = \frac{\partial}{\partial x}\left(\lambda_{ft}\frac{\partial T_f}{\partial x}\right) - \rho_o c_o v_f \frac{\partial T_f}{\partial x} + g^{(E)} \tag{2}$$

and in a low-permeability reservoir (in the region of the fracture to the reservoir boundaries)

$$\phi_m \beta_{mt} \frac{\partial P_m}{\partial t} = \frac{\partial}{\partial x}\left(\frac{k_m}{\mu_o}\frac{\partial P_m}{\partial x}\right) + \frac{\partial}{\partial y}\left(\frac{k_m}{\mu_o}\frac{\partial P_m}{\partial y}\right) \tag{3}$$

$$\alpha_{mt}\frac{\partial T_m}{\partial t} = \frac{\partial}{\partial x}\left(\lambda_{mt}\frac{\partial T_m}{\partial x}\right) + \frac{\partial}{\partial y}\left(\lambda_{mt}\frac{\partial T_m}{\partial y}\right) - \rho_o c_o\left(v_{mx}\frac{\partial T_m}{\partial x} + v_{my}\frac{\partial T_m}{\partial y}\right) + g^{(E)} \tag{4}$$

where P_f, T_f, P_m, and T_m are the pressure and temperature in the fracture and matrix, respectively, and ϕ_f, k_f, ϕ_m, and k_m are the porosity and permeability of the fracture and matrix, respectively. β_{ft} and β_{mt} denote the fracture and matrix total compressibility, and w_f is the fracture width. $C_{fD} = k_f w_f/k_m x_f$ is the dimensionless conductivity of the fracture. α_{ft}, λ_{ft}, α_{mt}, and λ_{mt} are the fracture and matrix total heat capacity and thermal conductivity, respectively. ρ_o and c_o are the density and specific heat capacity of oil, respectively. It is assumed that the height of the fracture equal to the thickness of the formation h and fracture characteristics are constant.

Fluid filtration in the fracture and matrix is described by Darcy's law.

$$v_f = -\frac{k_f}{\mu_o}\frac{\partial P_f}{\partial x}, \qquad v_{mx} = -\frac{k_m}{\mu_o}\frac{\partial P_m}{\partial x}, \qquad v_{my} = -\frac{k_m}{\mu_o}\frac{\partial P_m}{\partial y} \tag{5}$$

Oil viscosity is dependent upon the temperature as given by

$$\mu_o = \mu_{o,0}\exp(-\gamma_o(T - T_0)) \tag{6}$$

where $\mu_{o,0}$ is the value of viscosity at initial temperature $T = T_0$ and γ_o is the coefficient allowing for temperature dependence of the viscosity of oil.

It is assumed that the fracture and formation (matrix) are a homogeneous isotropic medium (with the same average parameters in relation to the electromagnetic field) saturated with hydrocarbon liquid (heavy oil). Heat sources in the formation and fracture are expressed by the following expression:[15]

$$g^{(E)} = -2\alpha_d J_b \frac{r_d}{r}\exp(-2\alpha_d(r - r_d)), \qquad J_b = N_0/S_b,$$
$$N_0 = N_g \exp[-2(\alpha_{d2} + \alpha_{d4})Z] \tag{7}$$

where α_d is the damping factor of the EM wave and $r = (x^2 + y^2)^{1/2}$. r_d denotes the radius of the EM wave radiator. r_w is the radius of the well. J_b is the intensity of the radiation EM wave, and $S_b = 2\pi r_d h$ is the area of the EM wave radiator. N_g and N_0 are the power of the EM wave generator and radiator, respectively, and Z is the reservoir depth. α_{d2} and α_{d4} are the damping factors of the EM waves in the tubing and casing.

The flow of oil from the reservoir (matrix) into the fracture is given by

$$q = -4\int_0^{x_f}\frac{k_m}{\mu_o}\frac{\partial P_m}{\partial y}\bigg|_{y=w_f/2}dx - 4\int_0^{w_f/2}\frac{k_m}{\mu_o}\frac{\partial P_m}{\partial x}\bigg|_{x=x_f}dy \tag{8}$$

2.2. Initial/Boundary Conditions and Stages. Initially ($t = 0$), "cold" oil production is carried out. The model is given initial pressure and temperature at the initial time and constant values at the boundaries of the reservoir.

$$P_m|_{t=0} = P_f|_{t=0} = P_i \tag{9}$$
$$P_m|_{y=L} = P_m|_{x=x_f+L} = P_i$$
$$T_m|_{t=0} = T_f|_{t=0} = T_0$$
$$T_m|_{y=L} = T_m|_{x=x_f+L} = T_0$$

Equations 1−4 are supplemented by the boundary conditions of the continuity of filtration and heat fluxes at the boundaries of "fracture−matrix", and boundary conditions are supplemented by the continuity of pressure and temperature.

$$\frac{k_f}{\mu}\frac{\partial P_f}{\partial y}\bigg|_{y=w_f/2} = \frac{k_m}{\mu}\frac{\partial P_m}{\partial y}\bigg|_{y=w_f/2}, \qquad P_f|_{y=w_f/2} = P_m|_{y=w_f/2},$$
$$\frac{k_f}{\mu}\frac{\partial P_f}{\partial x}\bigg|_{x=x_f} = \frac{k_m}{\mu}\frac{\partial P_m}{\partial x}\bigg|_{x=x_f}, \qquad P_f|_{x=x_f} = P_m|_{x=x_f} \tag{10}$$

$$\lambda_{ft}\frac{\partial T_f}{\partial y}\bigg|_{y=w_f/2} = \lambda_{mt}\frac{\partial T_m}{\partial y}\bigg|_{y=w_f/2}, \qquad T_f|_{y=w_f/2} = T_m|_{y=w_f/2},$$
$$\lambda_{ft}\frac{\partial T_f}{\partial x}\bigg|_{x=x_f} = \lambda_{mt}\frac{\partial T_m}{\partial x}\bigg|_{x=x_f}, \qquad T_f|_{x=x_f} = T_m|_{x=x_f} \tag{11}$$

In this case, a quarter of the model was considered because of the symmetry of the axis Ox (along the fracture) and the axis Oy (perpendicular to the fracture). Symmetry boundary conditions of pressure and temperature in the "fracture−matrix" set on the axes Ox and Oy

$$\frac{\partial P_f}{\partial x}\bigg|_{y=0} = 0, \qquad \frac{\partial T_f}{\partial x}\bigg|_{y=0} = 0, \qquad \frac{\partial P_m}{\partial x}\bigg|_{y=0} = 0,$$
$$\frac{\partial T_m}{\partial x}\bigg|_{y=0} = 0, \qquad \frac{\partial P_m}{\partial y}\bigg|_{x=0} = 0, \qquad \frac{\partial T_m}{\partial y}\bigg|_{x=0} = 0 \tag{12}$$

dx.doi.org/10.1021/ef5014264 | Energy Fuels 2014, 28, 5737−5744

It should be noted that the well radius (Figure 1) is much larger than the fracture width. However, the flow to the vertical well without fracture is much smaller than the flow along the fracture. Therefore, the size of the well in eqs 1−4 and the boundary conditions can be neglected [the well radius corresponds to the fracture width ($r_w \approx w_f/2$) in the mathematical model]. The boundary conditions (eq 13) characterize the current condition in the well and performed at the initialization fracture $x = r_w$, $y = r_w$. Constant bottom-hole pressure is given in the well and produces oil from the reservoir.

$$P_f|_{\substack{x=r_w \\ y=r_w}} = P_{wf}, \qquad \left.\frac{\partial T_f}{\partial x}\right|_{\substack{x=r_w \\ y=r_w}} = 0 \tag{13}$$

In the first stage, i.e., during "cold" production, the power of the RF−EM wave generator N_g is equal to 0 and Δt_1 is the duration of this stage. In the second, fourth, etc. stages, the oil production continues with simultaneous RF−EM irradiation (named as stages Δt_2, Δt_4, etc.) at relatively high temperatures. In the third, fifth, etc. stages, the "heated" oil is produced, while the EM wave generator is turned off ($N_g = 0$).

The flow rate of the oil is determined by

$$Q_w = 2hw_f\left[\frac{k_f}{\mu_o}\left.\frac{\partial P_f}{\partial x}\right|_{x=w_f/2} + \frac{k_m}{\mu_o}\left.\frac{\partial P_m}{\partial y}\right|_{y=w_f/2}\right] \tag{14}$$

We solved a two-dimensional (2D) problem numerically (eqs 3 and 4) in $0 \le x \le x_f + L$, $0 \le y \le L$. In the region ($0 \le x \le x_f$, $0 \le y \le w_f/2$), we used the properties of the fracture. In all other areas, the properties of the low-permeable matrix were defined. In this case, the conditions (eqs 10−11) are automatically satisfied.

In the numerical model, the fracture width is just one cell, which coincides with the width of the fracture. In cases of small width of fracture (w_f = 0.005 m) and a high-permeability fracture (k_f = 10−500 darcy), one cell to the fracture width was also sufficient. The gradients of dP/dy will not give significant differences to the simulation results, and to add additional cells to the width of the fracture will increase the computation time.

3. ANALYSIS OF NUMERICAL RESULTS

Equations 1−8 with the boundary conditions (eqs 9−13) were solved by the finite difference methods and with the iterative scheme of Newton's method. A non-uniform rectangular difference grid with decreased grid steps toward the fracture and boundaries was adaped. The total number of cells was 60 × 30. The simulation results were tested with the exact analytical solution for the case of isothermal flow to the fracture of finite conductivity in a single-porosity reservoir.[17] Simulations were performed with the parameters of the medium given in the Appendix. Damping factors of EM waves in the formation and fracture were assumed to be equal. The value α_d = 0.03267 m^{-1}, which is obtained when setting up a mathematical model for field tests, were used.[18]

Figure 2 shows the distribution of the temperature, viscosity, and inflow along the fracture at ΔP = 15 MPa, N_g = 20 kW, k_f =500 × 10^{-12} m^2, t_2 = 50 days, and different fracture half-lengths x_f = 5 and 10 m. High temperatures (up to 460 °C) and the greatest decrease in viscosity from 0.3 to 10^{-10} Pa s are observed in the near wellbore region (near the emitter EM wave). The larger the fracture length, the greater the rate to the well. Accordingly, more heat is carried away with the produced liquid from the reservoir and less heat will remain in the near wellbore. An increased temperature at the boundary of the fracture and formation is observed in the temperature profiles (Figure 2a). Increasing the temperature at the end of the fracture (at the boundary of the fracture and formation on the Ox axis) can be seen along the fracture. The temperature

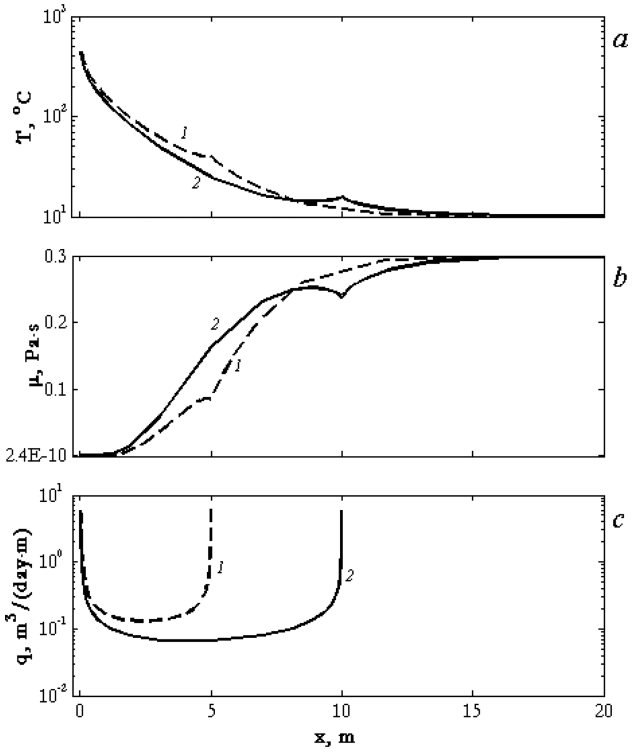

Figure 2. (a) Temperature, (b) viscosity, and (c) inflow of liquid distribution along the fracture at ΔP = 15 MPa, N_g = 20 kW, k_f = 500 × 10^{-12} m^2, t_2 = 50 days, and (1) x_f = 5 m and (2) x_f = 10 m.

increase at the end of the fracture (Figure 2a) causes a jump in fluid viscosity (Figure 2b). This temperature jump is explained by a significant difference in the rates of convective heat transfer in the fracture and formation and uneven inflow along the fracture. Inflow distribution along the fracture (Figure 2c) indicates that maximum inflow was observed at the end of the fracture.

Figure 3 shows the distribution of fluid inflow along the fracture at N_g = 20 kW, k_f = 500 × 10^{-12} m^2, x_f = 50 m, t_2 = 50 days,

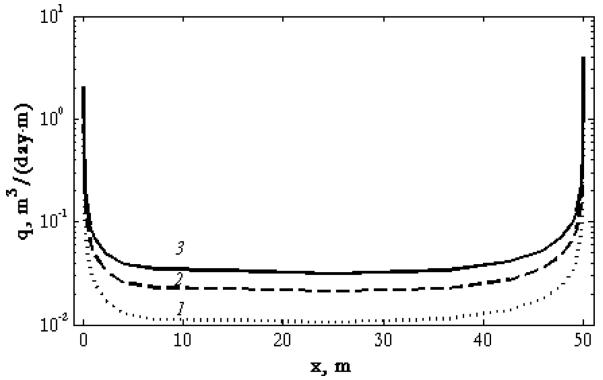

Figure 3. Inflow of liquid distribution along the fracture at N_g = 20 kW, k_f = 500 × 10^{-12} m^2, x_f = 50 m, t_2 = 50 days, and (1) ΔP = 5 MPa, (2) ΔP = 10 MPa, and (3) ΔP = 15 MPa.

and different pressures between the well and formation pressure (ΔP = 5, 10, and 15 MPa). The figure indicates a uniform inflow along the fracture (except near the wellbore and the end of the fracture). Inflow and pressure profiles along the fracture with a half-length of 50 m do not change substantially after 75 days of "cold" production.

dx.doi.org/10.1021/ef5014264 | Energy Fuels 2014, 28, 5737−5744

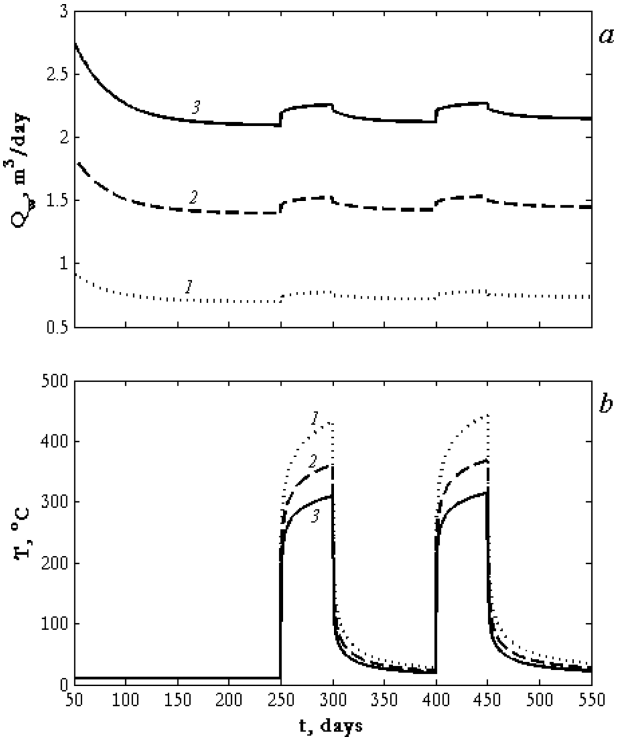

Figure 4. (a) Production rate dynamics and (b) temperature dynamics at the well at N_g = 20 kW, k_f = 500 × 10^{-12} m^2, x_f = 50 m, and (1) ΔP = 5 MPa, (2) ΔP = 10 MPa, and (3) ΔP = 15 MPa.

The behavior of the flow rate given in Figure 4 shows that, at $\mu_{o,0}$ = 300 × 10^{-3} Pa s, k_f = 500 × 10^{-12} m^2, and x_f = 50 m, the flow rate becomes a pseudo-steady state after ∼200 days. The second stage (the production of "heated" oil with RF−EM irradiation) starts after 250 days of "cold" oil production (Figure 4a). The temperature increases in the well (Figure 4b), resulting in an increase in the flow rate (Figure 4a) during the second stage. The greater the pressure differential between the well and the formation, the more heat is carried away with the heated fluid and the smaller the absolute value of the temperature in the borehole zone. Thus, the production rate (Figure 4a) and the liquid flow along the fracture (Figure 3) are substantially dependent upon the pressure differential between the well and formation. The adjustment of this pressure differential may reduce the undesirable high temperature, which eventually caused the forming of petroleum coke.

Figure 5 shows a comparison of the distributions of inflow along the fracture for the cases with a "cold" production (N_g = 0) and production with RF−EM heating at ΔP = 15 MPa, k_f =300 × 10^{-12} m^2, x_f = 10 m, and t_2 = 50 days. Obviously, the inflow profile along the fracture changed significantly with heating. The inflow to fracture at distances up to 2 m from the well is remarkably higher during the thermal influence of the RF−EM radiator than in the case of "cold" production. Inflow profiles along the fracture with increasing distances from the well differ slightly for both cases.

The oil rate (Figures 4a and 6a) and temperature (Figures 4b and 6b) change for k_f = 500 × 10^{-12} m^2, x_f = 50 m, and N_g = 20 kW at different pressure differentials between the well and formation (ΔP = 5, 10, and 15 MPa) and for k_f = 500 × 10^{-12} m^2, x_f = 50 m, and ΔP = 15 MPa at power EM wave generator (N_g = 0, 10, 20, and 30 kW) are shown in Figures 4 and 6, respectively. These figures indicate that the power generator of RF−EM waves and pressure differential between

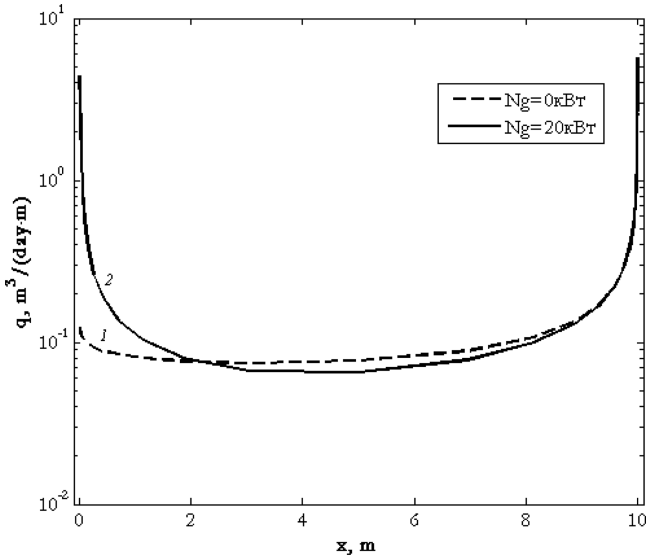

Figure 5. Inflow of liquid distribution along the fracture at ΔP = 15 MPa, k_f = 300 × 10^{-12} m^2, x_f = 10 m, t_2 = 50 days, and (1) N_g = 0 kW ("cold" production) and (2) N_g = 20 kW.

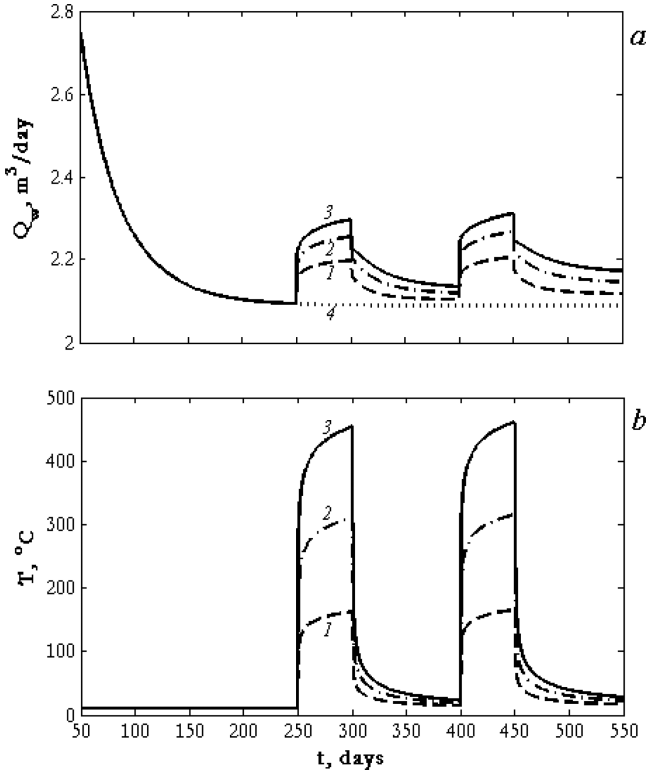

Figure 6. (a) Production rate dynamics and (b) temperature dynamics at the well at ΔP = 15 MPa, k_f = 500 × 10^{-12} m^2, x_f = 50 m, and (1) N_g = 10 kW, (2) N_g = 20 kW, (3) N_g = 30 kW, and (4) N_g = 0 kW ("cold" production).

the well and formation significantly affect the absolute values of the temperature in the borehole zone. The more power generator RF−EM waves and different pressure differentials between the well and formation, the more increase in the oil flow rate in the second and fourth stages (production with RF−EM heating). Reducing the oil flow rate and temperature in the well to the initial values (before RF−EM heating) was observed at the third and fifth stages of the production without RF−EM heating.

dx.doi.org/10.1021/ef5014264 | Energy Fuels 2014, 28, 5737−5744

The RF−EM generator is started in the second stage and then restarted in the fourth stage. Some of the heat in the borehole zone remained at the end of the third stage (production with off RF generator after heating). Figure 7 shows that the flow

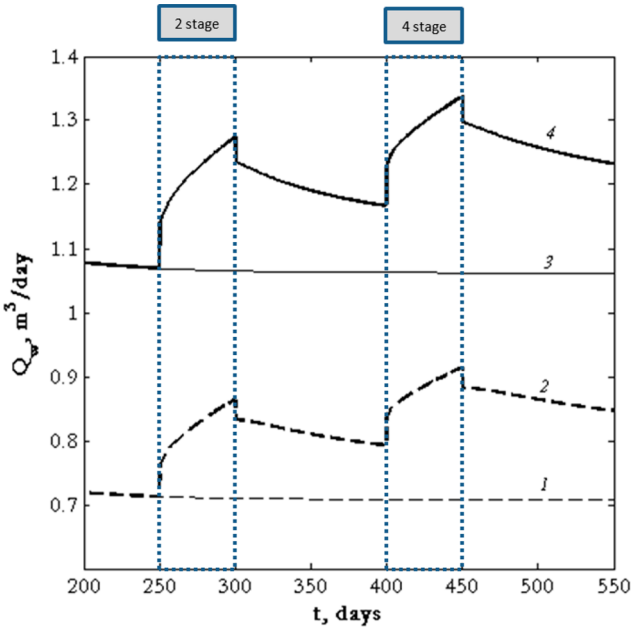

Figure 7. Production rate dynamics at (1 and 3) "cold" production N_g = 0 kW and (2 and 4) production with RF−EM heating N_g = 20 kW, at k_f = 300 × 10^{-12} m^2, x_f = 10 m, and (1 and 2) ΔP = 5 MPa and (3 and 4) ΔP = 10 MPa.

rate at the fourth and fifth stages is higher than that of the second and third stages (absolute values of the temperature in the well are also higher, as seen in Figures 4 and 6) because some of the heat remains in the borehole after the third stage. When oil production is compared for the cases with heating and "cold" production, one may observe that RF−EM heating provides additional oil production between 6 and 11% depending upon the differential pressure between the well and formation (Figure 7). Thus, in the case of a fracture with high conductivity and large half-length, greater convective heat transfer takes place. This takes a significant part of the heat produced along with heated oil from the formation.

The simulation results also indicate that power generator RF−EM waves can give undesirably high temperatures (above 300 °C). This level of temperature may result in phase transition, eventually yielding coke formation in the near wellbore zone. When the power generator of EM waves was adjusted, the differential pressure between the well and formation can be regulated and the negative effects of high temperatures in the near wellbore region can be prevented.

3.1. Simulation of Production/RF−EM Heating for "Short" Fractures. Figure 7 shows the dynamics of the oil rate at the "cold" production and production with RF−EM heating for differential pressure between the well and formation of 5 and 10 MPa. In this case (in comparison to the case of a fracture half-length of 50 m in Figure 6), additional production at all stages (with start and stop of the RF generator) is noticeable. In the case of production with RF−EM heating with a fracture length of x_f = 10 m, substantially more heat is retained than in the case with a fracture length of x_f = 50 m. An increased production of additional oil at the end of stage 5 is about 1.6 times larger than that of stage 3 in both cases, with a pressure between the well and formation of 5 and 10 MPa.

Figure 8 shows a comparison of the "cold" production and production with RF−EM heating for different power RF−EM

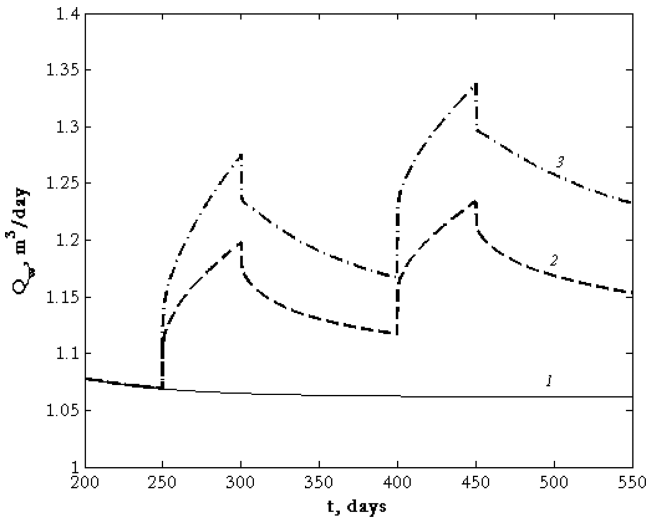

Figure 8. Production rate dynamics at the k_f =300 × 10^{-12} m^2, x_f = 10 m, ΔP = 15 MPa, and (1) "cold" production N_g = 0 kW and (2 and 3) production with RF−EM heating N_g = 10 and 20 kW.

wave generator. One may observe that the greatest increase in the oil rate compared to the "cold" production occurs at the end of the fifth stage. Additional production at the end of the fifth stage for the fracture half-length of 10 m and k_f = 300 × 10^{-12} m^2 (curves 1 and 3 in Figure 8) is about 3 times more than that for the half-length of 50 m and k_f = 500 × 10^{-12} m^2 (curves 2 and 4 in Figure 6). If the power of RF generator is N_g = 10 kW, the current oil rate is about 16% higher than that of "cold" production oil rate at the end of stage 5; it is about 26% when N_g = 20 kW.

Figure 9 compares the oil rates for "cold" production and production with the heating for different permeabilities of

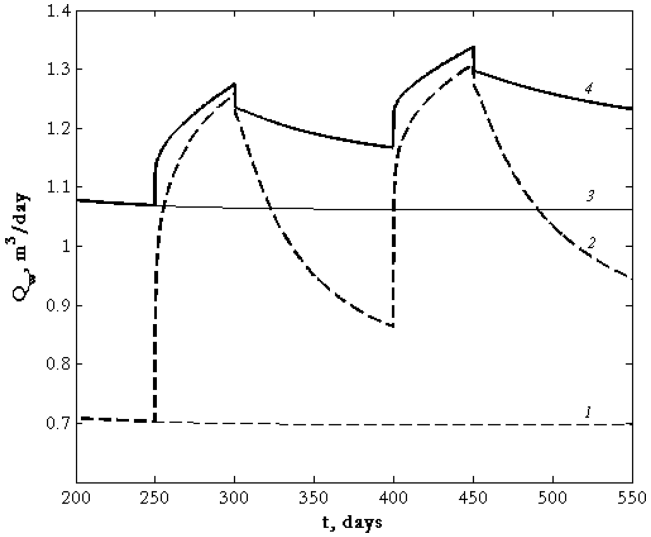

Figure 9. Production rate dynamics at the x_f = 10 m, ΔP = 15 MPa, (1 and 3) "cold" production N_g = 0 kW and (2 and 4) production/RF−EM heating N_g = 20 kW, and (1 and 2) k_f = 10 × 10^{-12} m^2 and (3 and 4) k_f = 300 × 10^{-12} m^2.

dx.doi.org/10.1021/ef5014264 | Energy Fuels 2014, 28, 5737−5744

the fracture. The figure shows that a significant amount of heat remains in the area around the well at low permeability of the fracture, which marked a significant difference in the production rate dynamics. The increase in oil production compared to the "cold" production at the end of the fourth stage is 26% for k_f = 300 × 10^{-12} m^2 and 87% for k_f = 10 × 10^{-12} m^2.

As previously noted, additional oil production decreases when the fracture half-length increases. Figure 10 shows a comparison of the curves of oil production/RF−EM heating and "cold" production at different fracture half-lengths. If x_f = 5 m, then the oil rate is about 52% higher than that of the "cold" production oil rate at the end of the fourth stage (with heating) and about 29% higher at the end of the fifth stage (off RF generator). This values are about 13 and 6% at the end of the fourth and fifth stages for x_f = 25 m.

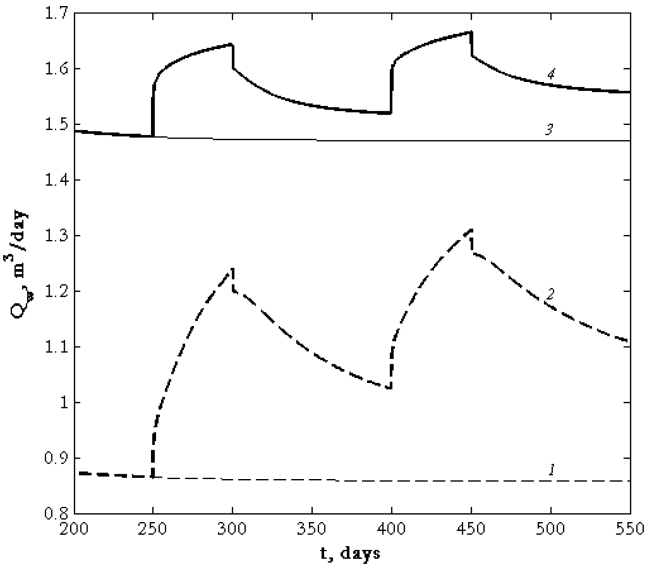

Figure 10. Production rate dynamics at k_f = 300 × 10^{-12} m^2, ΔP = 15 MPa, (1 and 3) "cold" production N_g = 0 kW and (2 and 4) production with RF−EM heating N_g = 20 kW, and (1 and 2) x_f = 5 m and (3 and 4) x_f = 25 m.

3.2. Comparison of Technology and Simple Economic Analysis. Figures 4 and 6−10 show a comparison of the production oil rate curves for the two cases: case 1, "cold" production of heavy oil in the fractured production well, and case 2, multi-stage production/RF−EM heating in the fractured well. We performed a sensitivity analysis on the production oil rate curves for the power of RF−EM wave generator, pressure differences between the well and formation, half-length, and permeability of the fracture. Analysis of the production data showed that the technology of production/RF−EM heated leads to a significant increase in oil production in the case of the "short" half-length fracture. In other cases, the heat from the reservoir goes along the production heated oil, and therefore, an increase in oil production is insignificant. Further, for the analysis of economic efficiency, cases with "short" fractures were considered.

An economic analysis was performed to compare multi-stage technology in this paper (case 2) with "cold" production (case 1). The cost of the RF−EM generator was assumed to be U.S. $100 000. The oil price was taken as $100/bbl in the calculations. The additional oil for case 2 was calculated as the difference between the cumulative oil produced by multi-stage production for 550 days (stages 1−5) with RF−EM heating and the cumulative "cold" heavy oil production for 550 days from the fractured well.

Payback times are given in Tables 1−4 for cases with different pressure differences between the well and formation (Table 1), power of RF−EM wave generator (Table 2), half-lengths of the fracture (Table 3), and fracture permeability (Table 4). For example, at a power of N_g = 10 kW, the cost of the RF−EM generator compensated after 54 months, and at N_g = 30 kW, it is 23 months. Analysis of the data shows that multi-stage technology is more effective for "short" half-length fracture and fracture with low permeability. Evaluating the effectiveness of this work does not consider the reduction of costs for cleaning wells from paraffins (low temperatures in the well), etc. The economic calculations should be regarded as an approximate estimate to give insight into the practicality of the

Table 1. Comparison of Cases for Different Reservoir/Bottom-Hole Differential Pressures

technology/cases	x_f (m)	k_f (mD)	ΔP (MPa)	N_g (kW)	Q (ton)	additional oil production (ton)	financial payback period (months)
"cold" production/multi-stage RF−EM treatment	10	300	5	0/20	200.2/222.5	22.3	69
			10		400.5/438.7	38.2	40
			15		600.7/650.2	49.5	31

Table 2. Comparison of Cases for Different Generator Performance Settings

technology/cases	x_f (m)	k_f (mD)	ΔP (MPa)	N_g (kW)	Q (ton)	additional oil production (ton)	financial payback period (months)
"cold" production	10	300	15	0	600.7		
multi-stage RF−EM treatment				10	629.2	28.5	54
				20	650.2	49.5	31
				30	666.8	66.1	23

Table 3. Comparison of Cases for Different Lengths of Fractures

technology/cases	x_f (m)	k_f (mD)	ΔP (MPa)	N_g (kW)	Q (ton)	additional oil production (ton)	financial payback period (months)
"cold" production/multi-stage RF−EM treatment	5	300	15	0/20	479.2/562.1	82.9	18
	10				600.7/650.2	49.5	31
	25				846.2/878.0	31.8	48

dx.doi.org/10.1021/ef5014264 | Energy Fuels 2014, 28, 5737−5744

Table 4. Comparison of Cases for Different Permeabilities of Fractures

technology/cases	x_f (m)	k_f (mD)	ΔP (MPa)	N_g (kW)	Q (ton)	additional oil production (ton)	financial payback period (months)
"cold" production/multi-stage RF−EM treatment	10	10	15	0/20	384.3/494.1	109.8	14
		50			518.2/592.3	74.2	21
		300			600.7/650.2	49.5	31

Table A1. Parameters of the Medium

symbol	parameter	value	unit
α_d	damping factor of EM wave	0.03267	m^{-1}
$\alpha_{d,t2}$	damping factors of the EM waves in the tubing	4.7755×10^{-4}	m^{-1}
$\alpha_{d,t4}$	damping factors of the EM waves in the casing	2.6048×10^{-4}	m^{-1}
α_{ft}	fracture total heat capacity	1487000	J m^{-1} K^{-1}
α_{mt}	matrix total heat capacity	1326000	J m^{-1} K^{-1}
β_{ft}	fracture total compressibility	1.03×10^{-8}	Pa^{-1}
β_{mt}	matrix total compressibility	1.83×10^{-9}	Pa^{-1}
C_{fD}	dimensionless conductivity of the fracture	0.1, 0.5, 1, 3, 5, 10, 25, and 50	
c_o	specific heat capacity of oil	2000	J kg^{-1} K^{-1}
k_f	permeability of the fracture	10×10^{-12}, 50×10^{-12}, 100×10^{-12}, 300×10^{-12}, and 500×10^{-12}	m^2
k_m	permeability of the matrix	10×10^{-15}	m^2
h	height of the fracture and thickness of the formation	10	m
$\mu_{o,0}$	value of viscosity at initial temperature	300×10^{-3}	Pa s
N_g	power of EM wave generator	0, 10, 20, and 30	kW
L_x	distance to the formation boundaries	100	m
L_y	distance to the formation boundaries	50	m
P_0	initial pressure	200×10^5	Pa
T_0	initial temperature	10	°C
r_d	radius of EM wave radiator	0.06	m
x_f	fracture half-length	5, 10, 25, and 50	m
w_f	fracture width	5×10^{-3}	m
Z	reservoir depth	2000	m
ϕ_f	porosity of the fracture	0.41	fraction
ϕ_m	porosity of the matrix	0.18	fraction
γ_o	coefficient allowing for temperature dependence of the viscosity of oil	0.042	K^{-1}
λ_{ft}	fracture total thermal conductivity	1.8274	W m^{-1} K^{-1}
λ_{mt}	matrix total thermal conductivity	2.4852	W m^{-1} K^{-1}
ρ_o	density of oil	950	kg/m^3
ΔP	pressure difference between the well and reservoir	5, 10, and 15	MPa
Δt_1	duration of the first stage	250	days
Δt_2 and Δt_4	durations of the second and fourth stages	50	days
Δt_3 and Δt_5	durations of the third and fifth stages	100	days

application. Note that not all parameters were duly taken into account in this exercise.

4. CONCLUSION

(1) Modeling of heavy oil production with RF−EM heating fractured showed that, after 50 days of RF−EM influence, there is an increase in the current oil rate production compared to the "cold" production; up to 87% in the end of stages 2 and 4. This is the greatest effect (increasing well production) observed for cases with "short" fractures and low permeability of fracture. (2) Fracture parameters, setting pressure, and power RF−EM generator can adjust the temperature in the system of "well fracture formation" by numerical modeling to predict oil production and prevent unwanted growth temperature in the well. (3) If there is no possibility of steam injection and/or the use of other methods of heavy oil production (e.g., because of the low-permeability reservoir), this technology may enable the production of heavy oil from low-permeability reservoirs with heavy oil. (4) It should be noted that additional oil production because of thermal expansion of oil[19,20] and heat loss to the surrounding rock[8] is not considered in this study. The positive contribution of the former and the negative impacts of the latter require further efforts, and this is the ongoing part of the research.

APPENDIX: INITIAL DATA

Parameters of the medium are given in Table A1.

AUTHOR INFORMATION

Corresponding Author

*E-mail: tayfun@ualberta.ca.

Notes

The authors declare no competing financial interest.

ACKNOWLEDGMENTS

This is an improved version of an abstract-based paper presented at the PetroPhase 2013, 14th International Conference on

Petroleum Phase Behavior and Fouling, June 10−13 2013, IFP Energies nouvelles, Rueil-Malmaison, France. This work was supported by an RFBR grant (14-01-97005) and a grant from the Ministry of Education and Science of Russia.

REFERENCES

(1) Chistyakov, S. I.; Sayakhov, F. L.; Babalyan, G. A. Experimental investigation of the dielectric properties of the formation under radio-frequency electromagnetic fields. *Univ. Invest.: Geol. Explor.* **1971**, *12*, 153−156.

(2) Sayakhov, F. L. Features filtration and fluid flow under the influence of radio frequency electromagnetic field. *Phys.-Chim. Hydrodyn.* **1982**, 108−120.

(3) Chakma, A.; Jha, K. N. Heavy-oil recovery from thin pay zones by electromagnetic heating *Proceedings of the 67th Annual Technical Conference and Exhibition of the Society of Petroleum Engineers*; Washington, D.C., Oct 4−7, 1992; SPE Paper 24817.

(4) Kasevich, R. S.; Price, S. L.; Faust, D. L.; Fontaine, M. F. Pilot testing of a radio frequency heating system for enhanced oil recovery from diatomaceous earth. *Proceedings of the 69th Annual Technical Conference and Exhibition*; New Orleans, LA, 1994; SPE Paper 28619.

(5) Ovalles, C.; Fonseca, A.; Lara, A.; Alvarado, V.; Urrecheaga, K.; Ranson, A.; Mendoza, H. Opportunities of downhole dielectric heating in Venezuela: Three case studies involving medium, heavy and extra-heavy crude oil reservoirs. *Proceedings of the International Thermal Operations and Heavy Oil Symposium and International Horizontal Well Technology Conference*; Calgary, Alberta, Canada, 2002; SPE Paper 78980.

(6) Nigmatulin, R. I.; Sayakhov, F. L.; Kovaleva, L. A. Cross transport phenomena in disperse systems interacting with a high-frequency electromagnetic field. *Dokl. Phys.* **2001**, *46* (3), 215−218.

(7) Davletbaev, A.; Kovaleva, L. A.; Nasyrov, N. M. Numerical simulation of injection of a solvent into a production well under electromagnetic action. *Fluid Dyn.* **2008**, *43* (4), 583−589.

(8) Davletbaev, A.; Kovaleva, L. A.; Nasyrov, N. M. An investigation of the processes of heat and mass transfer in a miltilayer medium under conditions of injection of a miscible agent with simultaneous electromagnetic stimulation. *High Temp.* **2009**, *47* (4), 574−579.

(9) Kovaleva, L.; Davletbaev, A.; Babadagli, T.; Stepanova, Z. Effects of electrical and radio-frequency electromagnetic heating on the mass-transfer process during miscible injection for heavy-oil recovery. *Energy Fuels* **2011**, *25* (2), 482−486.

(10) Bogdanov, I. I.; Torres, J. A.; Corre, B. Numerical simulation of electromagnetic driven heavy oil recovery. *Proceedings of the 18th SPE Improved Oil Recovery Symposium*; Tulsa, OK, April 14−18, 2012; SPE Paper 154140-PP.

(11) Carrizales, M. A.; Lake, L. W.; Johns, R. T. Multiphase fluid flow simulation of heavy oil recovery by electromagnetic heating. *Proceedings of the SPE Improved Oil Recovery Symposium*, Tulsa, OK, April 24−28, 2010; Paper SPE-129730-MS.

(12) Koch, A.; Sotskiy, S.; Mustafina, D.; Danov, V. Mechanism of heavy oil recovery driven by electromagnetic inductive heating. *Proceedings of the SPE Heavy Oil Conference-Canada*; Calgary, Alberta, Canada, June 11−13, 2013; Paper SPE-165507-MS.

(13) Trautman, M.; Macfarlane, B. Experimental and numerical simulation results from a radio frequency heating test in native oil sands at the North Steepbank Mine. *Proceedings of the 2014 World Heavy Oil Congress*; New Orleans, LA, March 5−7, 2014; Paper WHOC14-301.

(14) Hollmann, T. H.; Chapiro, G.; Heller, K.; Kermen, E.; Slob, E.; Zitha, L. J. EM stimulated water flooding in heavy oil recovery. *Proceedings of the 2014 World Heavy Oil Congress*; New Orleans, LA, March 5−7, 2014; Paper WHOC14-251.

(15) Abernethy, E. R. Production increase of heavy oils by electromagnetic heating. *J. Can. Pet. Technol.* **1976**, *15* (3), 91−97.

(16) Sayakhov, F. L. An investigation of thermal and hydrodynamic processes in multi-phase media affected by a radio-frequency electromagnetic field as applied to oil recovery. Dissertation of the Doctor of Physical and Mathematical Sciences, Lomonosov Moscow State University, Moscow, Russia, 1984; pp 469.

(17) Cinco-Ley, H.; Samaniego, V. F.; Dominguez, A. N. Transient pressure behavior for a well with a finite-conductivity vertical fracture. *SPE J.* **1978**, *6014*, 253−264.

(18) Davletbaev, A.; Kovaleva, L.; Babadagli, T. Mathematical modeling and field application of heavy oil recovery by radio-frequency. *J. Pet. Sci. Eng.* **2011**, *78* (3−4), 646−653.

(19) Burger, J.; Sourieau, P.; Combarnous, M. *Recuperation Assistee du Petrole les Methods Thermiques*; Editions Technip: Paris, France, 1984.

(20) Galimov, A. Yu.; Khabibullin, I. L. Features of high-viscosity fluid flow through a porous medium heated by electromagnetic radiation. *Fluid Dyn.* **2000**, *35* (5), 725−733.